

A High-Throughput Screening Pipeline to Identify Methyltransferase and Exonuclease Inhibitors of SARS-CoV-2 NSP14

Quinlin Hanson, Xin Hu, Sourav Pal, Katlin Recabo, Lin Ye, Ivy Poon, John-Paul Denson, Simon Messing, Min Shen, Kelli M. Wilson, Alexey Zakharov, Dominic Esposito, and Natalia J. Martinez*



Cite This: <https://doi.org/10.1021/acs.biochem.4c00490>



Read Online

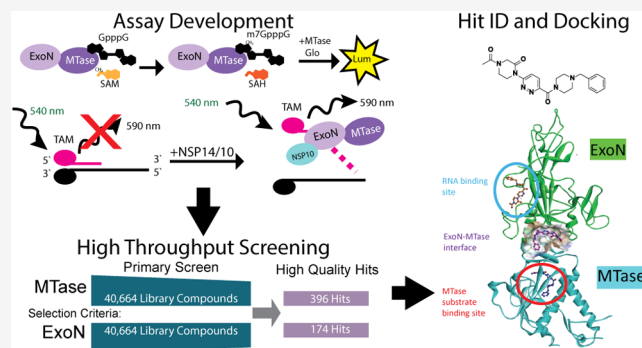
ACCESS |

Metrics & More

Article Recommendations

Supporting Information

ABSTRACT: SARS-CoV-2 infections led to a worldwide pandemic in 2020. As of 2024, therapeutics against SARS-CoV-2 have continued to be desirable. NSP14 is a dual-function methyltransferase (MTase) and exonuclease (ExoN) with key roles in SARS-CoV-2 genome propagation and host immune system evasion. In this work, we developed high-throughput screening (HTS) assays for NSP14 MTase and ExoN activities. We screened both activities against a collection of 40,664 compounds. A total of 1677 initial hit compounds were identified, cherrypicked, counterscreened for assay interference, and screened for off-target selectivity. We identified 396 and 174 high-quality hits against the MTase and ExoN activities, respectively. Along with inhibitors for individual activities, we identified dual-activity inhibitors, including a novel inhibitor that is not competitive with any substrate and interacts with a putative allosteric binding site. This study represents the largest published screen of SARS-CoV-2 NSP14 MTase and ExoN activities to date and culminates in a pipeline for the NSP14 drug discovery.



extensive contact with each other.⁷ However, catalytic dead mutations of either ExoN or MTase domain have no effect on the other's function.⁴

NSP14 forms a complex with the accessory protein NSP10.⁸ While the MTase activity is independent of NSP10 binding, the activity of the ExoN domain, which interacts directly with NSP10, is enhanced by NSP10. Structural studies have elucidated the mechanism for the enhancement of NSP14 ExoN by NSP10. Molecular dynamics simulations suggest the N-terminal region of the ExoN domain is disordered until NSP10 binds.⁸ Additionally, crystallography studies indicate that NSP10 binding moves key active site residues into the position for catalysis.^{7,8}

As a drug target, NSP14 is enticing, as both MTase and ExoN activities are important for viral viability. Catalytically dead mutants of either domain impair viral replication.⁴ Furthermore, the RdRp has a high mutation rate and readily incorporates incorrect nucleotides and nucleoside analogue

Received: August 22, 2024

Revised: December 23, 2024

Accepted: December 31, 2024

INTRODUCTION

Target-based approaches have proven successful in the development of current SARS-CoV-2 therapeutics. Nirmatrelvir, an M-pro inhibitor, and Molnupiravir and Remdesivir, RNA-dependent RNA-polymerase (RdRp) inhibitors, are currently FDA-approved to treat COVID-19. However, recent clinical trials concluded that Nirmatrelvir has no significant efficacy in adult patients who are at standard risk for severe COVID-19 or who are fully vaccinated and have at least one risk factor for severe COVID-19.¹ Hence, identification of inhibitors targeting other SARS-CoV-2 proteins remains an attractive effort.

NSP14 is a dual-function enzyme with 3'-5' exonuclease (ExoN) and N7-methyltransferase (MTase) activities.^{2–4} Both active site residues are highly conserved across coronaviruses.⁵ The N-terminal ExoN domain contains the classic DEDD motif present in the ExoN superfamily and confers proof-reading activity to compensate for the low fidelity of the viral RdRp.^{6,7} The C-terminal MTase domain is a SAM-dependent MTase which methylates the N7 of the 5'-guanine as the penultimate step in RNA capping.^{2–4} RNA capping protects viral RNA from degradation, helps evade host immunity, and aids in recruiting host elongation factors to promote translation of viral transcripts.^{2,3} The surface of the MTase domain is near the ExoN domain and both domains form

Table 1. Summary of Published Drug Discovery Efforts toward NSP14 ExoN or MTase Activities

reference	target	no. of compounds tested	assay method	hits	notes
Asthana et al. ¹²	ExoN	15 Dynasore analogues	HPLC	1	no MTase activity observed
Canal et al. ¹³	ExoN	5000 commercially available	FRET	12	
Rona et al. ¹⁵	ExoN	122 (2000 tested <i>in silico</i>)	FRET	23	structure-based design using molecular docking to select promising inhibitor candidates
Hernandez et al. ¹⁶	ExoN	113 metal chelators	fluorescence polarization	13	3 hits validated in cellular models
Ahmed-Belkacem et al. ¹⁸	MTase	31 SAH analogues	³ H radioactivity	13	hits based on IC ₅₀ determination
Ahmed-Belkacem et al. ¹⁷	MTase	39 SAH analogues	³ H radioactivity	7	3 hits provided thermal stability to NSP14
Hausdorff et al. ¹⁹	MTase	26 adenosine mimetics	³ H radioactivity	26	minor activity in Vero E6 TMPRSS2 cells
Otava et al. ²⁰	MTase	8 SAH derivatives	³ H radioactivity	8	
Samrat et al. ²¹	MTase	1584, NCI diversity set IV	fluorescence polarization	2	developed generalizable FP probe for MTases
Basu et al. ²²	MTase	5000, same as Canal et al.	HTRF	63	
Kasprzyk et al. ²³	MTase	7039 commercially available compounds, LOPAC, and FDA-approved drug library	fluorescence	83	3 inhibited viral replication in Huh 7 cells

^aHigh-throughput screening efforts.

drugs such as Remdesivir.^{2,3,10} ExoN is important for viral viability because it excises incorrectly incorporated nucleotides and protects against nucleoside analogues. Curiously, this dependence on the ExoN has also been observed in MERS-CoV, but to a lesser extent in SARS-CoV.⁵ The MTase domain also promotes viral viability by capping nascent RNA to protect from degradation and evade host immunity.^{2,3} One study suggests that the MTase function of exogenously expressed NSP14 is also responsible for triggering broad gene expression changes in cells, which are similar to those observed in SARS-CoV-2 infection.¹¹ Furthermore, fragment screening of NSP14 identified multiple “druggable” pockets, supporting that NSP14 is a target with potential for small molecule therapeutics.⁸

Indeed, prior efforts to identify inhibitors of NSP14 ExoN have been published (Table 1). Metal ejector/chelator compounds such as Patulin, HCV NSSA inhibitors, and analogues of Dynasore inhibit NSP14 ExoN activity with micromolar affinity.^{12–14} However, some of these studies employed approaches such as MALDI-MS, HPLC, or radioactivity-based methods, which are relatively low-throughput compared to 1536-well plate options and require relatively large amounts of sample per compound tested.^{4,12,14} On the high-throughput side of assays, Canal and colleagues screened 5000 compounds using a quenched-FRET assay.¹³ A similar assay was used to test 122 compounds, which were selected from a group of 10,000 virtually screened compounds.¹⁵ A fluorescence polarization assay, which is an HTS-amenable format, identified 9 inhibitors of NSP14 ExoN with micromolar IC₅₀ from a collection of 113 metal chelators.¹⁶

Efforts have also been dedicated to inhibitors of NSP14 MTase activity (Table 1). Several studies have detailed the structure-based design and synthesis of novel adenosine analogues and bisubstrate inhibitors targeting NSP14 MTase with nanomolar to micromolar affinity.^{17–20} These studies all employed a radioactivity-based method for measuring NSP14 MTase activity, which is sensitive and suitable for focused studies but not high-throughput amenable. A high-throughput fluorescence polarization assay was used to screen 1584 compounds from the NCI Diversity Set VI compound library and identified 2 hits.²¹ Similarly, a homogeneous time-resolved fluorescence (HTRF) assay was used to screen 5000

pharmaceutical compounds and identified compounds such as PF-03882845, Trifluperidol, Inauzhin, and Lomeguatibra as having micromolar activity toward NSP14 MTase.²² 83 compounds with IC₅₀ < 50 μM were identified from a set of 7039 compounds from commercially available library using an assay with a fluorescent probe, which mimics the MTase substrate.²³ While the above assays utilize fluorescent readouts, the MTase Glo system from Promega has also demonstrated use for viral MTase assays and general MTase assays.^{24,25}

In this work, we report the development of a high-throughput screening pipeline integrating both NSP14 MTase and ExoN assays in a 1536-well format. We incorporated counterscreening assays to remove compound-mediated assay interference as well as counterscreening assays for specificity using RNase H for ExoN and HNMT for MTase activity, respectively. Using this pipeline, we screened 40,664 compounds and identified hits with submicromolar inhibitory activity toward ExoN, MTase, and both functions. This study presents the largest and most comprehensive screen of drug-like compounds against both NSP14 MTase and ExoN activities to date.

METHODS

Reagents and Supplies. SARS-CoV-2 NSP14 (UniProtKB P0DTD1, positions 5926–6452) and HNMT (NCBI P50135.1) were procured from BioTechne (Minneapolis, MN). RNase H (cat. no. M0297, no accession given), GpppG (cat. no. S1407), me7GpppG (cat. no. S1404), GpppA (cat. no. S1406), and me7GpppA (cat. no. S1405) RNA cap analogues were procured from New England Biolabs (Ipswich, MA). Methylated RNA, me7CoV6 and me7Gen7, were produced by Bio-Synthesis (Lewisville, TX). All other RNA and DNA oligos, labeled and unlabeled, were produced by Integrated DNA Technologies (Coralville, IA). MTase Glo kit, which includes SAM, was procured from Promega (Madison, WI). White 384-well plates (medium binding, LUMITRAC, catalog no. 781075), black 384-well plates (medium binding, FLUOTRAC, catalog no. 781076), white 1536-well plates (medium binding, LUMITRAC, catalog no. 782075), and black 1536-well plates (medium binding, FLUOTRAC, catalog no. 782076) were procured from Greiner Bio-One (Monroe, NC).

Compound Libraries. Compound libraries were sourced from the National Center for Advancing Translational Sciences (NCATS) repositories (<https://ncats.nih.gov/research/research-activities/compound-management>). Libraries include: the NCATS Pharmaceutical Collection (NPC) 2.0, a library of annotated compounds that provide information on phenotypes, biological pathways, and cellular processes, and the Anti-Infectives Library.^{26,27} These libraries are referred to in the text as the “Annotated libraries”. The MiniPubChem and Genesis MiniMe collections are small, in-house libraries derived from the larger PubChem and Genesis collections of ~44,000 and ~100,000 diverse and medicinal chemistry-friendly compounds, respectively. These Mini collections are designed to preserve the chemical diversity of the large collections while streamlining the screening process (unpublished). The AI-Driven Library (AID) library is a new collection created in 2023 that is derived from multiple Enamine targeted libraries to generate a bespoke set of 6996 compounds with diverse biological indications (Figure S1). The MTase Collection is a commercial library of 11,000 compounds from ChemDiv (San Diego, CA).²⁵ For follow-up confirmatory assays, all compounds were sourced as fresh solutions from NCATS’ Compound Management. See the Assay Ready Plate Preparation section.

Generation of Expression Clones. SARS-CoV-2 nsp10-link-nsp14 clones were generated by DNA synthesis (ATUM, Inc., Newark, CA) with an optimized DNA sequence for bacterial expression in a Gateway Entry clone with an upstream TEV protease cleavage sequence (ENLYFQ/G) followed by amino acids 1–139 of SARS-CoV-2 nsp10 (UniProtKB entry P0DTD1, positions 4254–4392), a GGSGGS linker, and amino acids 1–527 of SARS-CoV-2 nsp14 (UniProtKB entry P0DTD1, positions 5926–6452). The Entry clone was subcloned into pDest-566 (Addgene #11517) to create a His6-MBP fusion protein for expression in *E. coli*.

SARS-CoV-2 nsp10 Entry clones were generated by amplification of DNA from a Midwest Structural Genomics Consortium nsp10 construct with an upstream TEV site containing additional linker amino acids (ENLYFQ/SNM) followed by amino acids 1–139 of SARS-CoV-2 nsp10. The Entry clone was subcloned into pDest-527 (Addgene #11518) to create a His6-fusion protein for expression in *E. coli*.

Protein Production. His6-tev-SARS-CoV-2 nsp10 was expressed in *E. coli* using the Dynamite medium protocol described previously.²⁸ In general, this is a complex medium which is a modification of Studier’s principles, that allows a higher final OD₆₀₀ after overnight induction with IPTG and incubation at 16 °C.²⁹ His6-MBP-tev-SARS-CoV-2 nsp10-link-nsp14 was expressed in *Vibrio natriegens* as described for the TBV2 protocol with modifications.³⁰ Specifically, the dissolved oxygen concentration was maintained at 40%. Both proteins were purified as described in Kopra et al., for KRAS4b (1–169) with exceptions.³¹ Specifically, for SARS-CoV-2 nsp10, the lysis buffer was 50 mM Tris (pH 8.0), 500 mM NaCl, 1 mM TCEP, and 1:100 protease inhibitor, and all other buffers (chromatography and final storage) were 50 mM Tris (pH 8.0), 500 mM NaCl, and 1 mM TCEP with the imidazole at 25 mM in the initial IMAC load. For SARS-CoV-2 nsp10-link-nsp14, the lysis buffer was 50 mM Tris-HCl (pH 7.5), 500 mM NaCl, 1 mM TCEP, 10% (v/v) glycerol, 0.05% (v/v) NP-40, 6 mM MgCl₂, RNase 0.42 µg/mL concentration (Cat# 70856, Millipore Sigma, Burlington, MA), Benzonase 130.5 units (Cat# 71205-3, EMD Millipore, Burlington, MA), and 1:200

protease inhibitor, and all other buffers (chromatography and final storage) were 50 mM Tris-HCl (pH 7.5), 500 mM NaCl, 10% (v/v) glycerol, 0.05% (v/v) NP-40, and 1 mM TCEP with the imidazole at 35 mM in the initial IMAC load. In general, the purification entails an IMAC step to capture the His6-tagged protein from the bacterial lysate, proteolytic cleavage of the His6-MBP N-terminal fusion with His6-TEV protease, isolation of the target protein by a second IMAC step, and a final size exclusion chromatography step. Final protein sequences are shown in the Supporting Information.

NSP10 + NSP14 Complex Formation. NSP10 + NSP14 complex was formed by incubating 0.5 µM NSP14 with 1.5 µM NSP10 in 20 mM Tris (pH 8.0), 50 mM NaCl, 3 mM MgCl₂, 0.1% Tween-20, and 0.1 mg/mL BSA at room temperature for 1 h. Complex formation was evaluated by comparing NSP14 ExoN activity to that of the NSP10+NSP14 complex. Complex concentrations are represented by the final concentration of NSP14 in each experiment.

Exonuclease Substrate Specificity and NSP10 Dependence. NSP14 ExoN substrate selectivity and NSP10 dependence were evaluated by comparing the exonuclease activity. Reactions were performed in 20 mM Tris (pH 7.5), 50 mM NaCl, 3 mM MgCl₂, 0.1% Tween-20, and 0.1 mg/mL BSA. In a black 384-well plate, 5 µL of 1 nM NSP10–14 fusion, NSP14, or NSP10+NSP14 complex was mixed with 5 µL of any of the following: 20 nM dsRNA substrate (5-TAM-G G U A G U A A U C C G C U - 3 with 5-UUUUUUUUUUUUUUUUUUUGAGCGGAUUA-CUACC-BHQ-3), dsDNA substrate (5-TAM-GGTAG-T A A T C C G C T - 3 with 5-TTTTTTTTTTTTTGAGCGGATTACTACC-BHQ-3), dTAM hybrid (5-TAM-GGTAGTAATCCGCT-3 with 5-UUUUUUUUUUUUUUUUUUUGAGCGGAUUA-CUACC-BHQ-3) or dBHQ hybrid (5-TAM-GGUAG U A A U C C G C U - 3 with 5-TTTTTTTTTTTTTGAGCGGATTACTACC-BHQ-3). Final reaction conditions were 0.5 nM enzyme and 10 nM oligonucleotide substrate. The reactions were incubated for 30 min at room temperature before reading TAMRA fluorescence (excitation 540 nm, emission 590 nm) on a Tecan Spark (Tecan Group, Männedorf, Switzerland) plate reader. Relative Fluorescence Units (RFU) of 3 replicates were plotted and compared to evaluate relative activity.

Methyltransferase Substrate Specificity and NSP10 Dependence. NSP14 MTase substrate specificity and NSP10 dependence were evaluated by comparing MTase activity using the MTase Glo assay kit. Reactions were performed in 20 mM Tris (pH 8.0), 50 mM NaCl, 3 mM MgCl₂, 0.1% Tween-20, and 0.1 mg/mL BSA. In white 384-well plates, 5 µL of 40 nM NSP14, NSP10–14 fusion, or NSP10 + NSP14 complex were combined with 6 µM SAM and 4 µM of one of the following substrates: GpppG cap analogue, me7GpppG cap analogue, GpppA cap analogue, me7GpppA cap analogue, CoV6 ssRNA (5-AGGGCU-3), me7CoV6 ssRNA (5-N7-Me-GpppAGGG-CU-3), Gen7 ssRNA (5-GpppACCCCC-3), or meGen7 ssRNA (5-N7-Me-GpppACCCCC-3). The final reaction concentrations were 20 nM enzyme, 3 µM SAM, and 2 µM substrate. Reactions were incubated at room temperature for 30 min, and then 2 µL of 5× MTase Glo Development reagent was added. This second reaction was incubated at room temperature for another 30 min, and then 12 µL of MTase Glo luciferase was added to the reaction followed by a final 30 min incubation. Luminescence was measured using a Viewlux plate

reader (PerkinElmer, Waltham, MA). Luminescence (AU) of 3 replicates was plotted and compared to evaluate relative activity.

DMSO Tolerance. DMSO tolerance for both NSP14 activities was assessed in 1536-well format as follows. DMSO at various volumes was transferred to 1536-well plates using an ECHO 655 acoustic liquid handler (Beckman, Indianapolis, IN). For ExoN activity, 2 μ L of NSP10–14 fusion protein in 20 mM Tris (pH 7.5), 50 mM NaCl, 3 mM MgCl₂, 0.1% Tween-20, and 0.1 mg/mL BSA, or buffer alone, was added to black 1536-well plates with DMSO. Then, 2 μ L of dsRNA substrate was added to initiate the reaction. The final reaction volume was 4 μ L with 0.5 nM NSP10–14 and 10 nM dsRNA substrate. Reactions proceeded for 10 min before reading TAMRA fluorescence on a Pherastar plate reader (BMG Labtech, Cary, NC).

For MTase DMSO tolerance, 2 μ L of NSP14 in 20 mM Tris (pH 8.0), 50 mM NaCl, 3 mM MgCl₂, 0.1% Tween-20, and 0.1 mg/mL BSA, or buffer alone, was added to white 1536-well plates with DMSO. Then, 2 μ L of GpppG cap analogue substrate with SAM was added to initiate the reaction. The final reaction volume was 4 μ L with 20 nM NSP14, 3 μ M SAM, and 2 μ M GpppG. Reactions proceeded for 30 min before adding MTase Glo reagents according to the manufacturer's instructions. Luminescence was read using a Viewlux plate reader.

ExoN K_M Determinations. To determine the K_M of NSP10–14 fusion and NSP14 + NSP10 complex for the ExoN dsRNA substrate (5'-TAM-GGUAGUAUCCGCU-3' with 5'-UUUUUUUUUUUUUUUUUGAGCGGAUUA-CUACC-BHQ-3') we used the method of initial rates. Briefly, in a black 384-well plate, dsRNA substrate was serially diluted 1:1 from 25 to 0.78 nM. 0.1 nM NSP10–14 fusion or the NSP14 + NSP10 complex was added to initiate the reaction. Reaction progress was monitored using a TECAN Spark plate reader measuring the TAMRA fluorescence (540 nm excitation, 590 nm emission) every minute for 45 min. Rates were determined from the linear region of each progress curve and plotted against the corresponding substrate concentration to generate a Michaelis plot. K_M values were determined by fitting data using the Michaelis–Menten equation.

NSP14 K_M Determinations. To determine the K_M of NSP14 MTase for the SAM cofactor and GpppG substrate, we used the method of initial rates. When determining the K_M for GpppG we titrated GpppG from 100 to 0.4 μ M while holding SAM constant at 200 μ M, and vice versa for determining the K_M for SAM. 10 nM NSP14 in 20 mM Tris (pH 8.0), 50 mM NaCl, 3 mM MgCl₂, 0.1% Tween-20, and 0.1 mg/mL BSA were added to each concentration of SAM/GpppG. Because reaction progress cannot be continuously monitored using MTase Glo, we initiated the reaction at distinct time points (0, 10, 20, 30, 40, 45, 50, and 55 min) and then added the MTase Glo Development reagent at the same time. This resulted in measuring pre-MTase Glo time points of 5, 10, 15, 20, 30, 40, 50, and 60 min. Rates were determined from the linear region of each progress curve and plotted against the corresponding substrate concentration to generate a Michaelis plot. K_M values were determined by fitting data using the Michaelis–Menten equation.

Assay Ready Plate Preparation. Assay Ready Plates (ARPs) were prepared by using a Beckman Access System (Beckman Coulter, Brea, CA). The acoustic dispense protocols were made by using Echo Plate Reformatted software. These

protocols were then implemented with Tempo scheduling software. The ARPs, as well as the sealed source plates (Beckman 1536-well low-dead-volume microplate, Echo Qualified; cat. no. LP-0400-BC) were loaded into a Thermo Scientific Cytomat24 (Thermo Fisher, Waltham, MA). A Precision SCARA robotic arm within the Access System transported the plates among various integrated instruments within the Access system. Source plates were peeled (Azenta XP-A XPeel, Azenta, Billerica, MA) before being placed in an Echo 655 (Beckman Coulter, Brea, CA) for a full plate survey. The ARP was transported from the Cytomat24 to the Echo destination stage, and a 20 nL 1:1 transfer was completed. Controls were dispensed from a Beckman 384-well low-dead-volume microplate (Echo Qualified; Cat# LP-0200-BC). The completed ARPs, source plates, and control plate were all sealed at 170 °C for 1.4 s (Agilent Technologies PlateLoc, Santa Clara, CA) and then returned to the Cytomat24. ARPs were placed in a –80 °C freezer until they were needed for the assay.

Screening Assay. Primary library screening was done in ARPs using the top 3 doses of each compound library. Before screening, ARPs were removed from the –80 °C freezer and brought up to ambient temperature on a benchtop over several hours. Cherrypicked compounds were replated into acoustic source plates and tested in an 11-point dose response. An Echo 655 acoustic liquid handler was used to dispense compounds for cherrypick assays. For ExoN all screening was done using the following protocol: In black 1536-well plates, 2 μ L of 1 nM NSP10–14 fusion was transferred to columns 1–2, 4–48 using a BIORATPR liquid handler. NSP10–14 was preincubated with compounds for 15 min. Then, 2 μ L of 20 nM dsRNA substrate was transferred to columns 1, 3–48. The negative control columns 3 and 4 were filled with assay buffer to have an equal volume, 4 μ L, as all other wells. Final reaction conditions were 0.5 nM NSP10–14, 10 nM dsRNA substrate in 20 mM Tris (pH 7.5), 50 mM NaCl, 3 mM MgCl₂, 0.1% Tween-20, and 0.1 mg/mL BSA. ExoN reaction proceeded at room temperature for 10 min before measuring TAMRA fluorescence (540 nm excitation, 590 nm emission) of each plate on a Pherastar plate reader (flying mode, gain value calibrated to 50% using column 1). Signal was normalized to the high signal wells in columns 1 and 2 and the negative control column 3, which contained dsRNA only and had a higher background than protein-only column 4. The counter-screen was performed using 1 nM TAMRA-labeled RNA in place of the RNA duplex. RNase H specificity screening was performed using 2.5 pM RNase H and 10 nM 5'-TAMRA-DNA/RNA-BHQ-3' hybrid duplex. Assaying timing and buffer were the same for each assay.

MTase screening was performed in white 1536-well plates. 2 μ L of 40 nM NSP14 was dispensed into columns 1–2, 4–48 of plates containing compounds. NSP14 was incubated with compounds for 15 min at room temperature. Then, 2 μ L of 4 μ M GpppG with 6 μ M SAM was transferred to columns 1–3, 5–48 of the same plate. 2 μ L of assay buffer was backfilled into negative control columns 3 and 4. Final reaction conditions were 20 nM NSP14, 2 μ M GpppG, 3 μ M SAM in 20 mM Tris (pH 8.0), 50 mM NaCl, 3 mM MgCl₂, 0.1% Tween-20, and 0.1 mg/mL BSA. MTase reaction proceeded for 30 min, then 1 μ L of 5X MTase Glo reagent was dispensed to each well by BIORATPR. This second reaction proceeded for 30 min at room temperature, then 5 μ L of MTase Glo luciferase reagent was added to each well using a Multidrop Combi with a

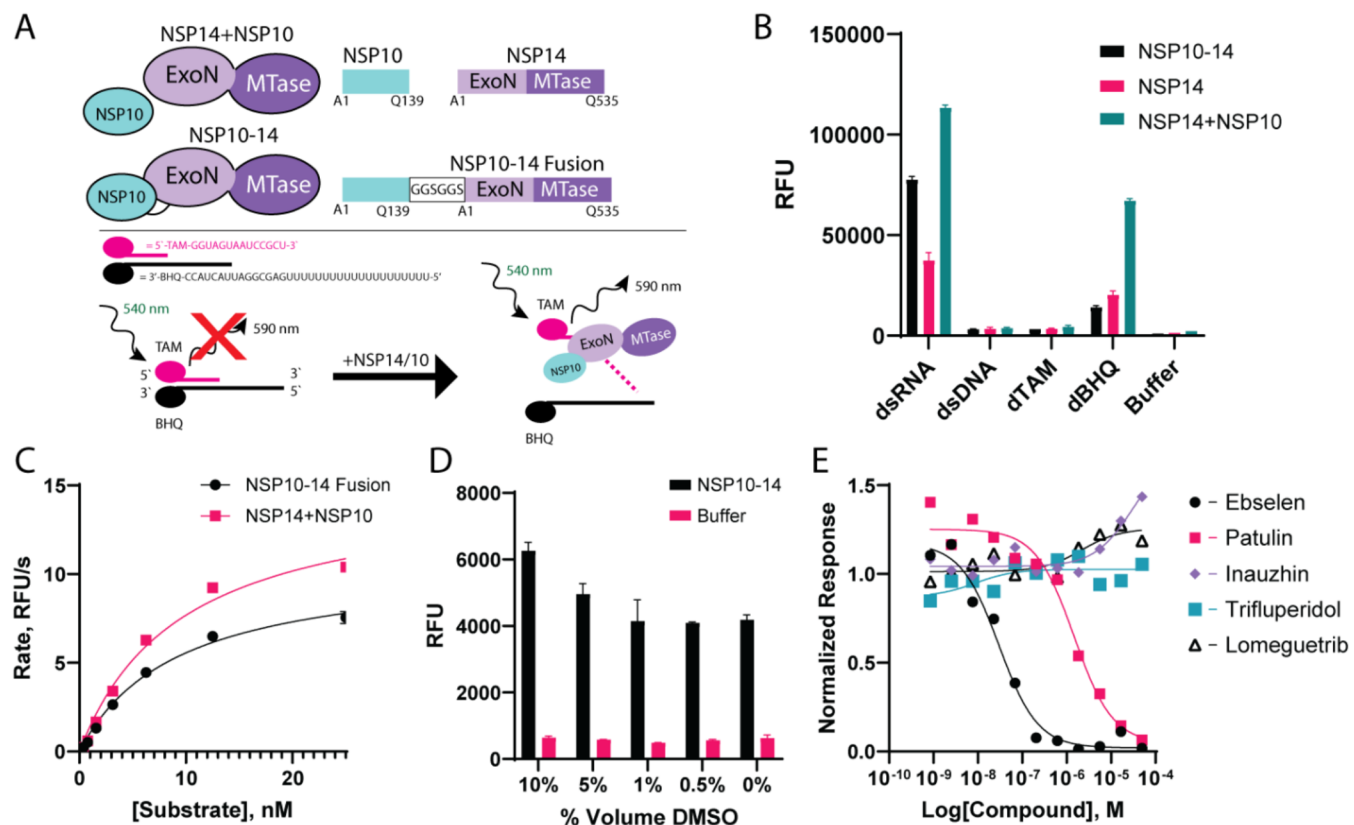


Figure 1. NSP14 Exonuclease (ExoN) Assay Development. (A) NSP14 ExoN assay was developed for the NSP10–14 fusion construct and NSP14 + NSP10 complex using a quenched-FRET strategy. A small 5'-TAMRA oligo is complexed with a longer 3'-BHQ strand, which quenches the fluorescence signal from TAMRA. NSP14 digests the 5'-TAM strand, releasing it from the quencher strand and leading to a signal increase over time. (B) The NSP10–14 fusion and NSP14+NSP10 complex showed a preference for dsRNA activity over dsDNA or hybrid complexes (dTAM and dBHQ). NSP10 improves the ExoN activity of NSP14 in both complexed and fusion forms ($n = 3$). Activity was determined by incubating 0.5 nM of the respective enzyme or enzyme complex with 10 nM substrate and then reading TAMRA fluorescence after 30 min of incubation at room temperature. (C) Michaelis constants for NSP10–14 fusion and the NSP14+NSP10 complex were determined by the method of initial rates. Similar K_m values were determined for NSP10–14 (9.2 ± 0.9 nM) and NSP14+NSP10 complex (9.6 ± 1.3 nM) ($n = 3$). (D) NSP10–14 tolerates DMSO well beyond the 0.5% used for screening assays ($n = 32$). DMSO tolerance was determined by the same methods used in (B). (E) Prior art inhibitors of NSP14 were assayed in dose response against 0.5 nM NSP10–14, 10 nM RNA duplex substrate, after 10–20% product conversion (10 min).

standard dispensing cassette (Thermo Fisher, Waltham, MA). Plates were incubated at room temperature for 30 min, and then the luminescent signal was read on a Viewlux plate reader. Signal was normalized to the high signal wells in columns 1 and 2 and the negative control columns 3 and 4. The MTase Glo counterscreen was performed similarly, but the 20 nM NSP14 solution was replaced with a 400 nM SAH solution. Similarly, the HNMT specificity screen was performed using 7.5 nM HNMT instead of NSP14, and the substrate solution used 5 μ M histamine and 6 μ M SAM. The same buffer and timing were used for all assays.

Compound Structure Clustering. Structural clustering was performed with TIBCO Spotfire version 11.4.4 (TIBCO Software Inc., Palo Alto, CA). The process begins with preparing the chemical structure data, followed by generating molecular fingerprints ECFP4 (Extended Connectivity Fingerprints) that capture key structural elements. A similarity matrix is then created using the Tanimoto coefficient to quantify pairwise molecular similarity. Hierarchical clustering using a UPGMA algorithm is applied to assign compounds to clusters based on their structural likeness. The resulting structure clusters were visualized through a dendrogram, enabling examination of cluster relationships and identification of key

structural patterns. Clusters were refined by adjusting similarity thresholds to 0.5 to ensure that compounds with identical core structures were grouped together, reducing the effects of large or complex R-groups. Structure–activity relationships were visualized using a heatmap to represent the compound activity against NSP14 ExoN and MTase activities.

Inhibitor Mechanism Studies. NCGC00537446 mechanism for NSP10–14 ExoN was determined as follows. A 2X stock of 0.7 nM NSP10–14 was preincubated with compound at 0.16, 0.5, 1.5, or 4.4 μ M, or just DMSO in 20 mM Tris (pH 7.5), 50 mM NaCl, 3 mM MgCl₂, 0.1% Tween-20, and 0.1 mg/mL BSA for 30 min. A 2X stock of FRET paired RNA duplex was serially diluted from 400 to 6 nM. 5 μ L of each NSP10–14 + drug combination was mixed with 5 μ L of each substrate concentration in a black 384-well plate, and reaction progress was monitored for 60 min using a TECAN Spark (ex: 535 nm, em: 590 nm). Initial rates were extracted from the linear region of the progress curve. For each compound concentration, a Michaelis–Menten and Lineweaver–Burk plot was generated. K_m and V_{max} values were determined from each plot and graphed as a function of compound concentration.

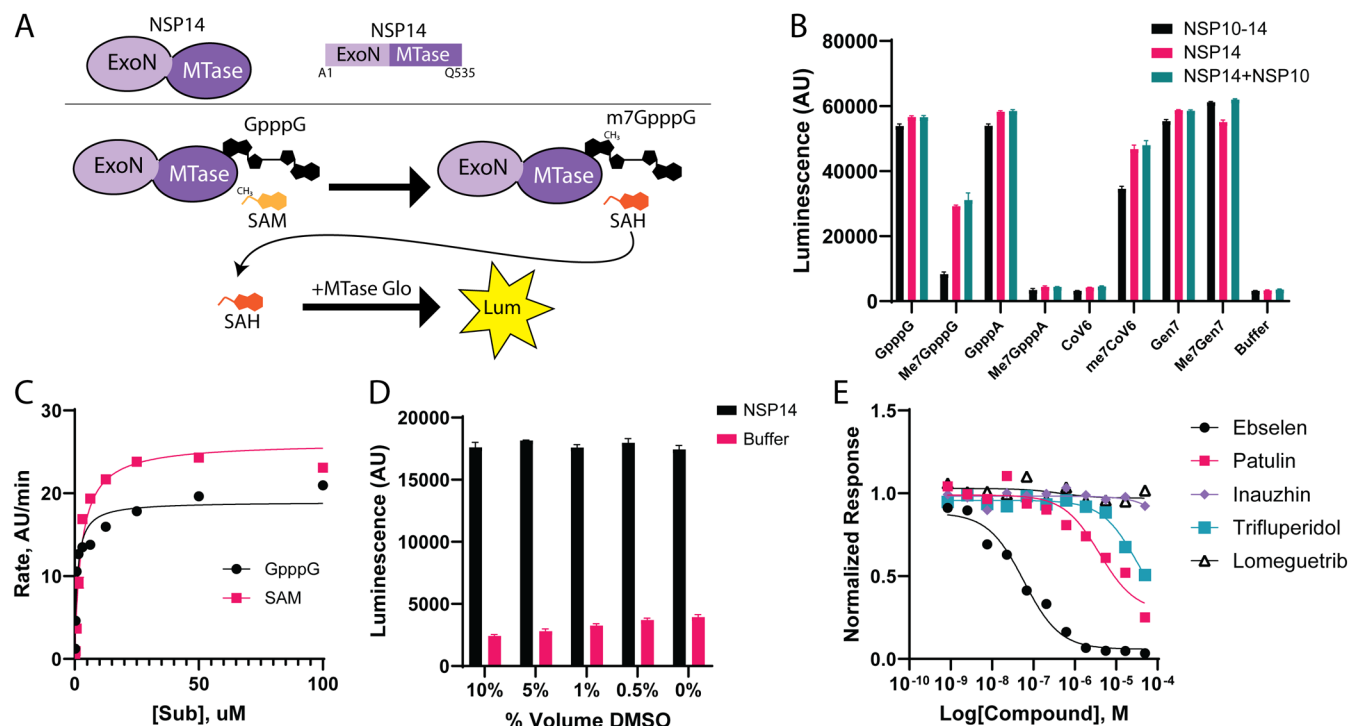


Figure 2. NSP14 methyltransferase (MTase) assay development. (A) NSP14 MTase uses a GpppG cap analogue as the substrate and SAM as the methyl donor. (B) NSP14 MTase activity is independent of NSP10. 10 nM enzyme or enzyme complex was reacted with 3 μM SAM and 2 μM of the indicated substrate for 60 min. MTase activity was measured using the MTase Glo Kit, which generates a luminescent signal proportional to SAM conversion. (C) Michaelis constants for GpppG ($1.04 \pm 0.14 \mu\text{M}$) and SAM ($2.65 \pm 0.27 \mu\text{M}$) were determined using the method of initial rates ($n = 3$). For GpppG K_M determination, SAM was held constant at 200 μM. For SAM K_M determination, GpppG was held constant at 200 μM. (D) NSP14 MTase activity tolerates DMSO well above the 0.5% used for screening assays ($n = 16$). DMSO tolerance was determined for the SAM/GpppG substrate using the same method as (B). (E) Reported NSP14 inhibitors (Ebselen, Patulin, and Trifluperidol) were tested in dose response against 10 nM NSP14, 3 μM SAM, and 2 μM GpppG. Reactions were performed at room temperature for 30 min, then SAM was converted to a luminescent signal using MTase Glo following the manufacturer's protocol.

NCGC00537446 mechanisms for NSP14 MTase were determined as follows. When the mechanism was determined with respect to GpppG, SAM was held constant at 100 μM and vice versa. A 2× stock of GpppG or SAM was serially diluted from 50 to 0.4 μM in 20 mM Tris (pH 8.0), 50 mM NaCl, 3 mM MgCl₂, 0.1% Tween-20, and 0.1 mg/mL BSA. 2 μL of the solutions were distributed to a white 1536-well plate using a BIORAPTR. 10, 7.5, 5, 2.5, 1, 0.5, and 0.1 μM of compound or DMSO were acoustically transferred to the same plate. A 2× stock of 40 nM NSP14 in the same buffer was prepared. To initiate the MTase reaction, 2 μL of the enzyme solution was transferred by BIORAPTR to discrete sections of the 1536-well plate at 0, 15, 30, 40, 50, and 60 min time points to discontinuously monitor reaction progress. After the final time point, SAH was converted to luminescence using an MTase Glo (Promega, Madison, WI). Initial rates were extracted from the linear region of the progress curve. For each compound concentration and Michaelis–Menten and Lineweaver–Burk plot was generated. K_M and V_{max} values were determined from each plot and graphed as a function of compound concentration.

Molecular Docking. Three protein structures of Nsp14 in complex with different substrates or ligands were retrieved from the Protein Data Bank: 7QIF (in complex with a methylated GpppG at the MTase active site), 7N0B (in complex with RNA and Nsp10 at the ExoN domain), and 5SKW (in complex with a small molecule inhibitor at the ExoN-MTase domain interface). Prior to docking, the protein

structures were processed using the Structure Preparation Module in the MOE program (www.chemcomp.com). Docking studies of inhibitor NCGC00537446 to the different binding sites at the ExoN domain (7N0B), the MTase domain (7QIF), and the domain interface (5SKW) were performed using the MOE Dock, respectively. The ligand-induced fit docking protocol was applied, and binding affinity was evaluated using the GBVI/WSA score. The top-ranked binding poses from each docking were inspected, and the predicted inhibitor binding complexes at the three binding sites were further minimized and rescored.

Data Analysis and Graphics. All screening data and cherrypicked assay data were uploaded to an in-house database using in-house tools. Data analysis for identifying hits and selecting follow-up compounds was performed using in-house tools and TIBCO Spotfire version 11.4.4 (TIBCO Software, Inc., Palo Alto, CA). PCA calculations were performed in KNIME (KNIME, Inc., Austin, TX), and plots were generated in seaborn.³² All other graphs were generated in GraphPad Prism version 10.0.2 (GraphPad Software, Boston, MA). Structure clustering and heat maps were generated with TIBCO Spotfire. All figures were assembled in Adobe Illustrator (Adobe, Inc., San Jose, CA).

RESULTS

A Nsp14 MTase/ExoN Dual-Activity HTS Assay Pipeline. Our goal was to develop a high-throughput screening (HTS) pipeline to identify inhibitors of NSP14 ExoN and

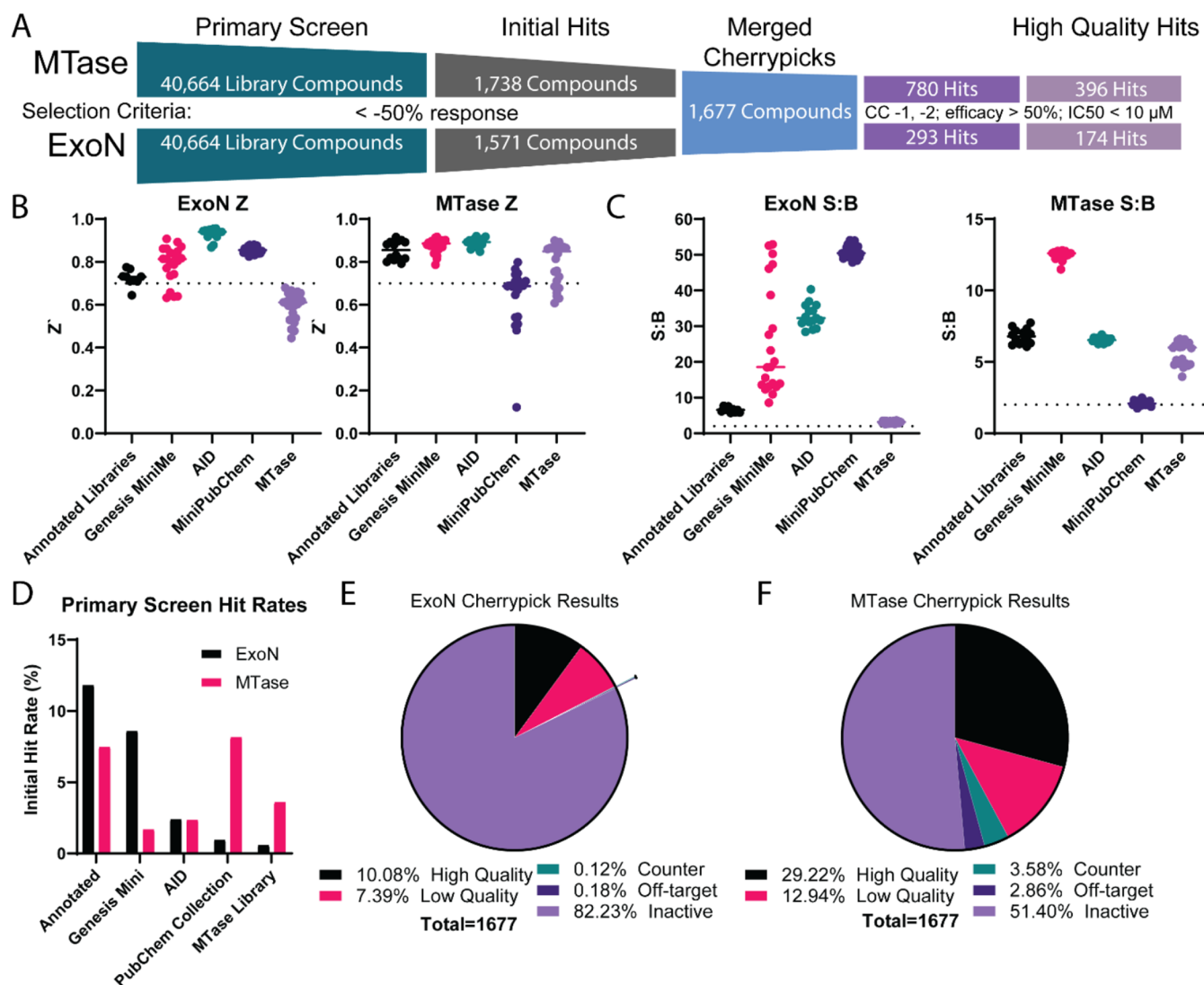


Figure 3. NSP14 screening overview and results. (A) Screening funnel for NSP14 MTase and ExoN assays. 40,664 library compounds were screened in 3- or 4-point dose response. Those with at least -50% max response (50% inhibition) were cherrypicked for validation and tested in an 11-point dose response. Validated hits were defined as those compounds with a curve class of -1 or -2 , efficacy of -50% , and $\text{EC}_{50} \leq 10 \mu\text{M}$. (B) Z' values for ExoN and MTase primary screening. The dashed line indicates $Z' = 0.7$, which is the ideal cutoff for biochemical assays. Each dot represents a single 1536-well plate from the given compound library. (C) Signal-to-background (S:B) for primary screening results. The dashed lines indicate an S/B cutoff of at least 2. (D) Hit rates for primary screening indicating what % of compounds from each library were initial hits. (E, F) Cherrypick and validated hits for NSP14 HTS. High-quality hits are those with curve class of -1 or -2 , efficacy of -50% , and $\text{EC}_{50} \leq 10 \mu\text{M}$. Low-quality hits are those which are not high-quality and show at least single-point dose response. Counter hits are compounds that were positive in the respective counter assays. Off-target hits are those that were active against RNase H for ExoN and HNMT for MTase. All of the other compounds were deemed inactive.

MTase activities. To achieve this, we designed HTS-amenable assays for both NSP14 activities. To monitor ExoN activity, we used quenched-FRET to report on RNA degradation by NSP14 ExoN (Figure 1A).^{13,15} NSP14 ExoN activity is enhanced by NSP10 when fused to the N-terminus of NSP14 and when complexed together as separate proteins (Figure 1B). Although the NSP14 + NSP10 complex had higher activity than the NSP10–14 fusion, the K_M value for the dsRNA substrate is similar between the NSP14 + NSP10 complex ($9.6 \pm 1.3 \text{ nM}$) and the NSP10–14 fusion ($9.2 \pm 0.9 \text{ nM}$) (Figure 1C). Therefore, we used the NSP10–14 fusion for HTS for ease of use. To ensure our assay would be suitable for HTS using compounds dissolved in DMSO, we tested NSP10–14 for DMSO tolerance and response to prior art inhibitors. DMSO comprises 0.5% of the total assay volume,

and NSP10–14 tolerates DMSO even at 10% of the final reaction volume (Figure 1D). Testing previously reported inhibitors of NSP14, we observed NSP14 ExoN inhibition by Patulin and Ebselen, but not for other reported NSP14 MTase inhibitors (Figure 1E).^{13,22} All of these features indicated that the NSP10–14 ExoN assay is suitable for HTS.

Additionally, we developed an assay to measure the NSP14 MTase activity. Our NSP14 MTase assay uses the MTase Glo kit (Promega, Madison, WI), which has been extensively used for screening of MTase enzymes^{24,25,33} (Figure 2A). NSP14 MTase acts on a variety of RNA substrates, as well as GpppG and GpppA cap analogues. NSP14 also showed activity on the methylated Me7GpppG cap analogue but not Me7GpppA. RNA substrates without any portion of the cap, like CoV6 (AGGGCU) were not methylated by NSP14, but RNAs such

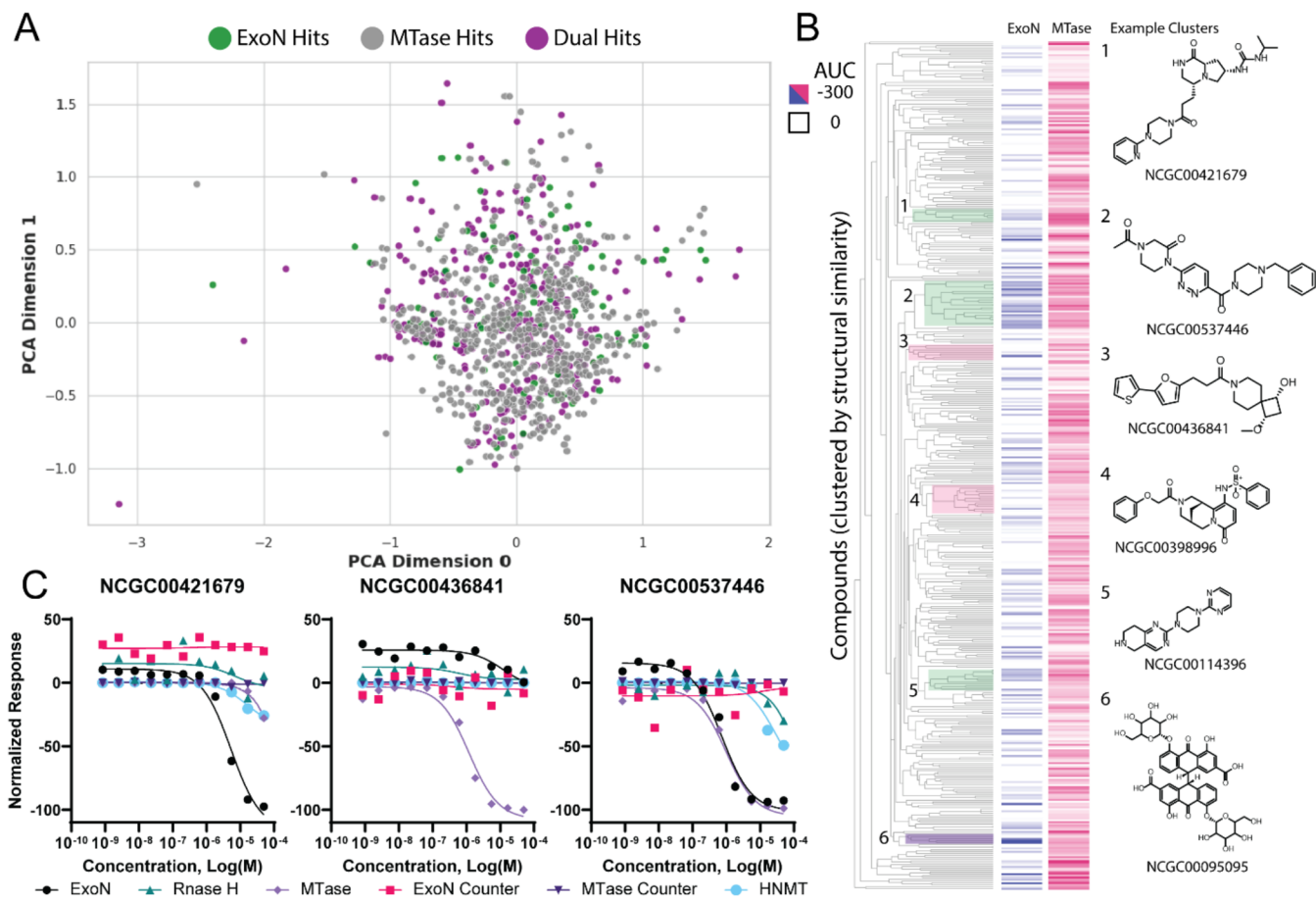


Figure 4. Analysis of the NSP14 hit compounds. Hit compounds from the NSP14 MTase pipeline were tested in the NSP14 ExoN assays and vice versa. (A) Principal component analysis of NSP14 hits. For this analysis, hits are defined as compounds with curve class -1 or -2. PCA dimensions describe chemical linkages and properties. Compounds are defined as ExoN Hits (green), MTase Hits (gray), or Dual Hits (purple). (B) Structure clustering of curve class -1 and -2 compounds along with their respective activity (AUC) toward NSP14 ExoN (blue) and MTase (pink). (C) Example hits of an ExoN specific, MTase specific, or dual-activity hit.

as me7CoV6 (me7GpppAGGGCU), Gen7 (GpppACCCCC), and me7Gen7 (me7GpppACCCCC) were methylated by NSP14, similar to previously reported studies (Figure 2B).³⁴ NSP10 had no influence on NSP14 MTase activity regardless of its presence in a fusion construct or complex (Figure 2B). However, with certain substrates, NSP10–14 fusion showed lower activity than NSP14 alone or the NSP14 + 10 complex. We wanted to ensure our MTase measurements were free from potential interference from ExoN activity. Thus, for assay development, we used NSP14 alone, which lacks ExoN activity, and the GpppG cap analogue substrate, which is not processed by the ExoN domain. We determined the K_m of NSP14 MTase for SAM ($2.65 \pm 0.27 \mu\text{M}$) and GpppG ($1.04 \pm 0.14 \mu\text{M}$) using the method of initial rates (Figure 2C). Like the ExoN assay, NSP14 MTase tolerated DMSO well above 0.5% used for HTS assays (Figure 2D). NSP14 MTase activity was inhibited by Patulin and Ebselen, similar to ExoN, both domains are sensitive to metal chelation (Figure 2E).³⁵ However, the reported EC₅₀ values for Inauzhin and Lomeguetrib, 23 and 59.8 μM , respectively, were near or above our highest dose tested of 40 μM and thus outside our assay window.²² These data indicate that the NSP14 MTase assay is suitable for HTS, the second of two needed assays to evaluate potential NSP14 inhibitors.

Library Screening for Inhibitors of Nsp14. To identify NSP14 inhibitors, we screened NSP14 MTase and ExoN

assays against a total of 40,664 compounds each (Figure 3A). These libraries comprised the Annotated Libraries (3448 compounds) as well as medchem-friendly compounds (37,216 compounds) from a selection of the Genesis and PubChem collections, (referred to as Genesis MiniMe, MiniPubChem Collection) the AID, and the MTase Library. Primary screening was done in 3- or 4-doses, depending on the plate formatting of the given library. Final concentrations of 40, 13.3, and 4.4 μM were screened for three-dose libraries. Four-dose libraries had an additional concentration at 1.48 μM . Compounds with at least -50% response (or 50% inhibition) at the top dose and -10% response for a second dose were defined as initial hits and cherrypicked for further testing. Cherrypicked compounds were replated from fresh compound stocks and retested in an 11-point dose response. Compounds that met the selection criteria (curve class -1, -2; efficacy >50%, IC₅₀ > 10 μM) were defined as high-quality hits.

Both assays performed well with $Z' > 0.7$ for most primary screening results (Figure 3B,C). However, the MTase library screen of NSP14 ExoN activity underperformed in the primary screen and initial hits were all manually verified due to noisy control columns. For the MiniPubChem screen of NSP14 MTase, some plates underperformed with low Z' values and low S:B, again likely due to noisy or poorly dispensed control columns. However, all libraries contained at least one high-dose plate surpassing the cutoff values of $Z' > 0.7$ and S:B > 2.

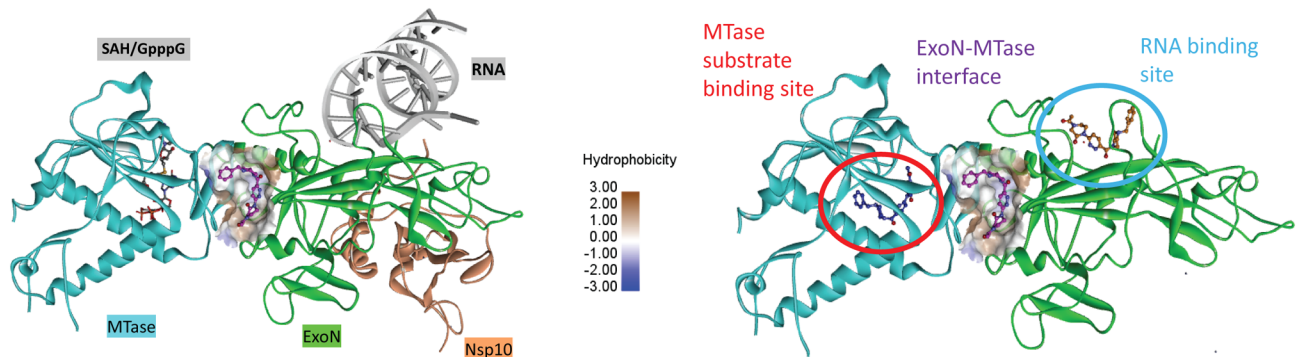
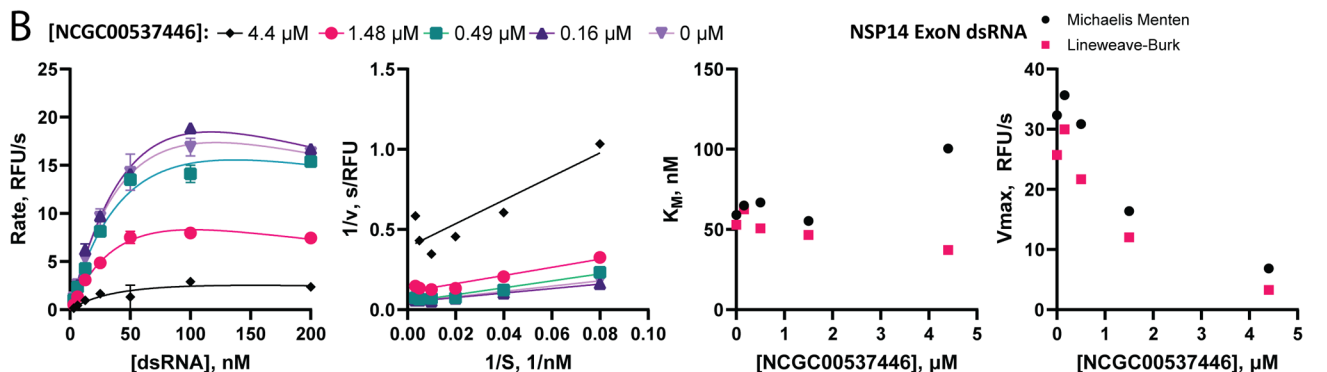
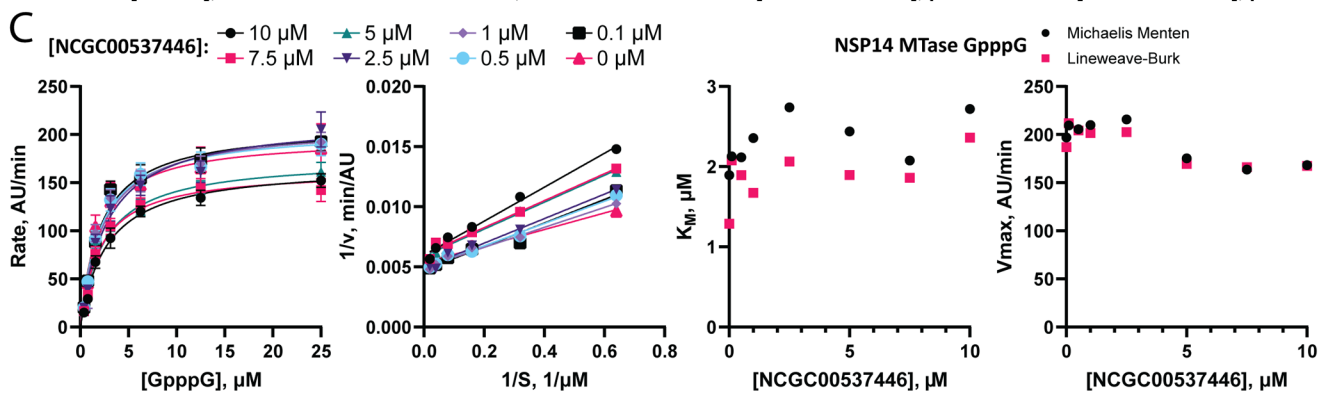
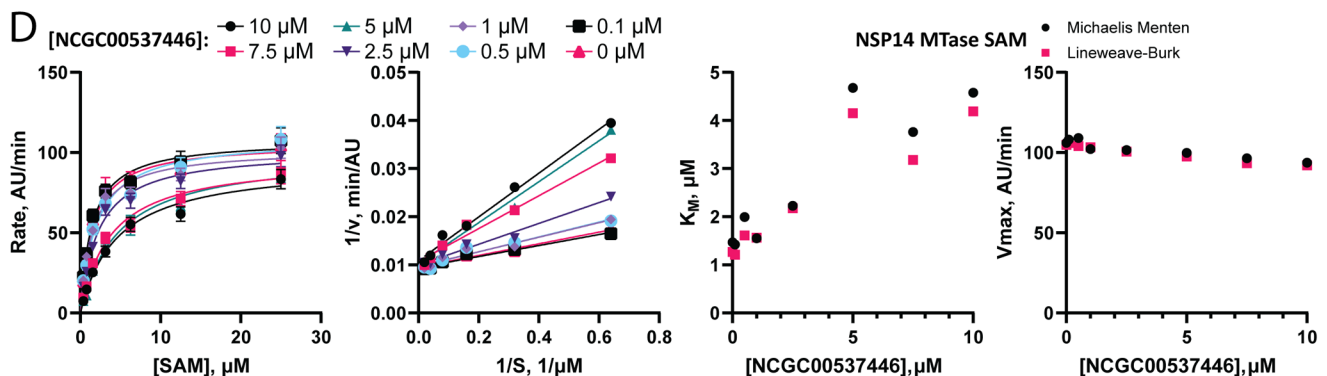
A**B****C****D**

Figure 5. Model of NSP14 inhibition by NCGC00537446. (A) Molecular docking of NCGC00537446 into a structure of NSP14. The structure presented is built from structures of NSP14 in complex with m7GpppG (PDB ID: 7QIF), in complex with RNA and NSP10 (PDB ID: 7N0B), and in complex with an inhibitor (PDB ID: 5SKW). Left: NCGC00537446 (purple sticks) docked at the interface of the ExoN and MTase domains. Right: Predicted binding models of inhibitor NCGC00537446 bound to NSP14 at the substrate binding site of the MTase domain, the RNA binding site at the ExoN domain, and the ExoN-MTase interface. Inhibitors are shown as sticks, and the protein surface at the interface pocket is shown in hydrophobicity. The docking scores are -7.75 (interface site), -7.59 (MTase substrate site), and -5.12 (RNA binding site) (B) Effect of NCGC00537446 on NSP10–14 ExoN activity. The left two plots are the Michaelis–Menten and Lineweaver–Burk plots, respectively. The right two plots are the derived K_M and V_{max} values plotted against inhibitor concentration. 2.5 μ M NSP10–14 was preincubated with NCGC00537446 at 0–4.4 μ M compound for 30 min. ExoN activity was initiated by adding 10 nM of duplexed RNA substrate and monitoring TAMRA fluorescence (ex: 535 nm, em: 590 nm) for an hour. Initial rates were determined, and Michaelis–Menten and Lineweaver–Burk plots were generated. K_M and V_{max} values were extrapolated from each plot and graphed as a function of NCGC00537446 concentration. (C, D) Effect of NCGC00537446 on NSP14 MTase activity with respect to GpppG (C) and SAM (D). The left two plots are the Michaelis–Menten and Lineweaver–Burk plots,

Figure 5. continued

respectively. The right two plots are the derived K_M and V_{max} values plotted against inhibitor concentration. GpppG and SAM were mixed with 0–10 μM compound and dispensed into 1536-well plates. MTase reactions were initiated by distributing 20 nM NSP14 to appropriate wells and progressed for 0, 10, 20, 30, 45, and 60 min. For GpppG experiments, SAM was held constant at 100 μM . For SAM experiments, GpppG was held constant at 100 μM . Once all reactions had been completed, SAH conversion was detected using MTase Glo. Initial rates were determined and Michaelis–Menten and Lineweaver–Burk plots were generated. K_M and V_{max} values were extrapolated from each plot and graphed as a function of NCGC00537446 concentration.

Initial hits were manually verified for all low-performing assays. The initial hit rates for ExoN and MTase assays differed across libraries (**Figure 3D**). NSP14 ExoN had highest initial hit rates from the Annotated Libraries and the Genesis Mini library. NSP14 MTase had a lesser, but still relatively high, hit rate for the Annotated Libraries as well as a higher hit rate for the MiniPubChem and MTase libraries.

Overall, we identified 1571 and 1738 initial hits for ExoN and MTase, respectively. A combined total of 1,677 compounds were available for cherrypicking and were replated to confirm activity. Of these initial hits, 293 and 780 confirmed ExoN and MTase inhibitory activity, respectively (**Figure 3E,F**). This relatively low confirmation rate is acceptable because we set loose initial hit criteria to promote the opportunity of identifying weaker hits for early SAR. Next, we filtered out assay artifacts by counterscreening for assay interference in the absence of enzyme. The ExoN assay tested compounds against dsRNA substrate alone to check for fluorescence interference while the MTase assay used compounds in the presence of 0.4 μM SAH to check for MTase Glo-interfering compounds. A small percentage of compounds (0.12 and 3.58% for ExoN and MTase, respectively), were identified as interfering and filtered out. Next, we tested for off-target effects using RNase H as our off-target exonuclease and HNMT as our off-target methyltransferase. For NSP14 ExoN, only 0.18% of hits were active against RNase H, while 2.86% of NSP14 MTase hits were active against HNMT (**Figure 3E,F**). The remaining hits were defined as high-quality hits (curve class -1, -2; efficacy >50%, EC₅₀ > 10 μM), low-quality hits (not high-quality and at least single-point activity), or inactive. The overall hit rate for NSP14 ExoN was lower than that for MTase, with 7.39% of cherrypicked compounds being defined as high-quality hits and 10.08% low-quality hits. NSP14 MTase had a relatively high hit rate, with 29.22% high-quality hits and 12.94% low-quality hits.

Detergent Tolerance of ExoN and MTase Assays. The NSP10–14 fusion construct required the presence of a detergent for activity in any assay format. Furthermore, pilot studies suggested that for our automated liquid handling systems, a large amount of detergent was required to maintain an active NSP10–14 enzyme. Therefore, our buffer system incorporated 0.1% Tween-20 into all of the buffers. However, this is a concentration above the CMC of Tween-20 with the potential to cause assay interference or false positives in our screening assay. To validate hits, we manually tested key hit compounds using 0.01% Tween-20, which, for this assay, is suitable for pipetting but not for automated liquid handling (**Figure S2**). We did notice prior art compounds, such as Sinefungin and Ebselen, displayed increased potency with higher detergent concentrations in NSP14 MTase but not in the NSP10–14 activity assay. No exemplar hits from our study showed significant shifts in activity with respect to the detergent concentration.

Structural Diversity of Identified Inhibitors of Nsp14.

To describe the chemical space of ExoN and MTase hits, we did a principal component analysis (PCA) on hit compounds (**Figure 4A**). We described compounds based on activity toward only NSP14 MTase, only NSP10–14 ExoN, or those with any activity toward both. 647 compounds were active against only MTase, 105 were active against only ExoN, and 346 compounds had dual activity. No significant clustering was observed in the PCA plot, suggesting similar chemical space is occupied by ExoN, MTase, and dual inhibitors. To further explore the properties of observed hits, we performed a structure-cluster analysis. Compounds were clustered by applying a UPGMA hierarchical clustering algorithm using the Tanimoto coefficient derived from ECFP4 molecular fingerprint to quantify pairwise molecular similarity. Clustering is visualized in a dendrogram with a heatmap indicating ExoN and MTase activities (**Figure 4B**). There are 80 clusters containing at least two compounds with a similarity score of 0.5 and 51 singlettons with no similar compounds. ExoN-selective clusters were rare in this data set. Cluster 1 contains the ExoN-selective compound NCGC421679, but many of the other members have dual activity based on the area under the curve (AUC) of the dose response curve (**Figure 4C**). Cluster 6 contains seven compounds enriched in polyphenols such as NCGC00095095 and tannic acid. MTase-selective clusters, such as clusters 3 and 4, are more common. The largest cluster of highly similar compounds is cluster 2, with 24 members that have overall high activity against both ExoN and MTase activities, such as NCGC00537446. Although there is some activity against non-NSP14 targets such as RNase H and HNMT, NCGC00537446 is over 10-fold more efficacious toward NSP14 making this an enticing cluster for further SAR profiling in the future.

Dual Nsp14 MTase/ExoN Inhibitor. Identifying the novel inhibitor NCGC00537446 with dual MTase/ExoN inhibitory activity is an unprecedented finding. We validated that the inhibition of NSP14 ExoN and MTase activity by NCGC00537446 was not due to assay interference via counterscreen and ruled out any detergent-driven inhibition mechanism by manually testing the assays with 0.01% Tween-20 or no detergent, where applicable (**Figure S2**). We were curious about the possible mechanism of inhibition that a dual inhibitor might employ to hit both activities. Toward this end, molecular docking was performed using three available NSP14 structures: 7QIF (NSP14 with Me7GpppG in the MTase active site), 7N0B (NSP14 in complex with NSP14 and RNA at the ExoN active site), and 5SKW (NSP14 in complex with a small molecule at the ExoN-MTase interface).^{8,36} NCGC00537446 was modeled into both active sites and the interface site with docking scores of -7.75 for the interface site, -7.58 for the MTase active site, and -5.12 for the ExoN active site (**Figure 5A**). Because the docking scores were similar for two sites, we decided to biochemically determine the mechanism of inhibition with respect to the ExoN RNA

substrate, the MTase GpppG substrate, and the MTase SAM cofactor (Figure 5B–D). For the ExoN RNA substrate, we observed no significant change in K_M value at concentrations below 2 μM NCGC00537446. At 4.4 μM the apparent K_M values depend on if the Michaelis–Menten plot or Lineweaver–Burk plot are used to extrapolate the value, although the Lineweaver–Burk fits are heavily skewed by apparent substrate inhibition (Figure 5B). V_{\max} is more clearly influenced by NCGC00537446 concentration, consistent with a noncompetitive model. With respect to the GpppG MTase substrate, K_M is not significantly influenced by NCGC00537446 while there is some influence on V_{\max} again consistent with a noncompetitive model (Figure 5C). Finally, with respect to SAM, NCGC00537446 increases the K_M by roughly 2-fold at 10 μM compound but has no influence on V_{\max} (Figure 5D). This is consistent with a competitive model of inhibition with respect to SAM. NCGC00537446 might have multiple modes of inhibition with respect to ExoN and MTase activity with an overall mixed method of inhibition.

■ DISCUSSION

Herein we report a pipeline for NSP14 ExoN and NSP14 MTase HTS. Within this study, we developed HTS assays in a 1536-well format for both NSP14 ExoN and MTase activities. Both assays perform well in the 1536-well format according to standard practices. They are also scalable to lower-throughput formats such as a 384-well, which is what we used for the initial assay development. The screening of 40,664 compounds represents the largest single screening effort against NSP14 ExoN and MTase activities to date. This work also comprises a curated data set suitable for *in silico* screening or launching further SAR development/screening campaigns. These data are publicly available on PubChem, providing broad access to a data set that is often beyond the scope of smaller research institutes.

From the set of 40,664 compounds, we identified 780 compounds with activity against NSP14 MTase, 396 of which were high-quality hits with EC₅₀ values <10 μM . For NSP14 ExoN we identified 293 hits with 174 of those hits being high quality. The dose response range tested, 40 μM to 677 pM, favors higher potency compounds. The formatting of our compound storage and liquid handling limits our highest concentration to near 40 μM . Thus, weaker hits with high micromolar potencies would not be detected in our assays, which explains why many reported inhibitors of NSP14 would not be detected in this assay system.^{18–23}

By investigating both activities, we identified a novel inhibitor of NSP14 with dual activity and a potentially complex mechanism of inhibition. We characterized the mechanism of one such inhibitor, NCGC00537446. With respect to ExoN activity, NCGC00537446 was noncompetitive or mixed with the exact mechanism being obfuscated by substrate inhibition. For MTase activity, it was noncompetitive with GpppG and competitive with SAM. Based on molecular docking, the most likely binding sites were the MTase active site and the ExoN-MTase interface, which were identified as potential drug binding sites fragment screening effort.⁸ Our docking models and mechanism studies together suggest that the SAM position of the MTase active site is the binding site of NCGC00537446, which would explain the inhibition of MTase activity. Regarding ExoN inhibition, we have two main hypotheses. First, is that allosteric communication between the MTase and ExoN domains leads to the inhibition

of NSP14 ExoN activity, likely because the two domains share an extensive interface.⁷ Second, NCGC00537446 also binds the ExoN-MTase interface in addition to the SAM binding site. A lesser hypothesis is that all three binding sites are viable, depending on whether the ExoN mechanism is noncompetitive or mixed. Further biophysical and structural studies are needed to address the details of how these dual inhibitors work.

It is worth noting that small off-target effects were observed for NCGC00537446. Although there was a greater than 10-fold potency difference between NSP14 ExoN and RNase H, and NSP14 MTase and HNMT, careful refinement of analogues and broader screening of off-target enzymes would need to be done to lower the risk of off-target effects. It is a novel finding to encounter a dual-activity inhibitor of NSP14 and this presents an opportunity to consolidate efforts to inhibit NSP14 ExoN and NSP14 MTase activities. Moving forward, we will pursue investigating some of these hit compounds in models of SARS-CoV-2 replication and infection. Furthermore, this data set can be expanded on through further SAR studies and analogue generation to improve on single-activity or dual-activity inhibitors.

■ CONCLUSIONS

SARS-CoV-2 NSP14 is a dual-function enzyme with MTase and ExoN activities. Inhibitors against either activity would be promising antiviral therapeutics. In this study, we developed 1536-well format HTS assays for SARS-CoV-2 NSP14 MTase and ExoN activities. Using these assays, we screened 40,664 compounds against both ExoN and MTase activities and identified 396 hits against the MTase activity and 174 hits against the ExoN activity. From these hits, we identified a unique compound, NCGC00537446, an inhibitor against both MTase and ExoN. Molecular docking studies identified putative binding sites in the MTase active site, the ExoN active site, and an allosteric site at the interface of the two functional domains. To investigate these models, we did inhibition mechanism studies that suggest a mixed mode of inhibition mediated through the SAM binding site and/or the allosteric site. In conclusion, NSP14 is a good target for SARS-CoV-2 antiviral drug development, and we identified a first-in-class, dual-activity, NSP14 inhibitor, NCGC00537446.

■ ASSOCIATED CONTENT

SI Supporting Information

The Supporting Information is available free of charge at <https://pubs.acs.org/doi/10.1021/acs.biochem.4c00490>.

AID library descriptors, detergent assays, and protein sequences (PDF)

Accession Codes

NSP10: UniProtKB P0DTD1, position 4254–4392. NSP14: UniProtKB P0DTD1, position 5926–6452. HNMT: NCBI PS0135.1. RNase H: NEB Cat # M0297, no accession given.

■ AUTHOR INFORMATION

Corresponding Author

Natalia J. Martinez — National Center for Advancing Translational Sciences, National Institutes of Health, Rockville, Maryland 20850, United States;
Email: natalia.martinez@nih.gov

Authors

Quinlin Hanson — National Center for Advancing Translational Sciences, National Institutes of Health, Rockville, Maryland 20850, United States;  [orcid.org/0000-0001-6033-8415](#)

Xin Hu — National Center for Advancing Translational Sciences, National Institutes of Health, Rockville, Maryland 20850, United States

Sourav Pal — National Center for Advancing Translational Sciences, National Institutes of Health, Rockville, Maryland 20850, United States

Katlin Recabo — National Center for Advancing Translational Sciences, National Institutes of Health, Rockville, Maryland 20850, United States

Lin Ye — National Center for Advancing Translational Sciences, National Institutes of Health, Rockville, Maryland 20850, United States

Ivy Poon — Protein Expression Laboratory, Cancer Research Technology Program, Frederick National Laboratory for Cancer Research, Frederick, Maryland 21701, United States

John-Paul Denson — Protein Expression Laboratory, Cancer Research Technology Program, Frederick National Laboratory for Cancer Research, Frederick, Maryland 21701, United States;  [orcid.org/0009-0004-1191-5641](#)

Simon Messing — Protein Expression Laboratory, Cancer Research Technology Program, Frederick National Laboratory for Cancer Research, Frederick, Maryland 21701, United States

Min Shen — National Center for Advancing Translational Sciences, National Institutes of Health, Rockville, Maryland 20850, United States;  [orcid.org/0000-0002-8218-0433](#)

Kelli M. Wilson — National Center for Advancing Translational Sciences, National Institutes of Health, Rockville, Maryland 20850, United States;  [orcid.org/0000-0003-2636-2766](#)

Alexey Zakharov — National Center for Advancing Translational Sciences, National Institutes of Health, Rockville, Maryland 20850, United States;  [orcid.org/0000-0003-2466-1711](#)

Dominic Esposito — Protein Expression Laboratory, Cancer Research Technology Program, Frederick National Laboratory for Cancer Research, Frederick, Maryland 21701, United States

Complete contact information is available at:

<https://pubs.acs.org/10.1021/acs.biochem.4c00490>

Author Contributions

Q.H. performed biochemical assays and screens; X.H., S.P., A.Z., and L.Y. performed data processing and deposition; X.H., A.Z., and M.S. designed AID library; K.R. performed compound plating; I.P., S.M., J.-P.D., and D.E. produced recombinant proteins; Q.H., X.H., and S.P. created figures; N.J.M. supervised the project; Q.H. and N.J.M. performed data analysis and wrote the manuscript.

Funding

This work was supported by the intramural research program of the National Center for Advancing Translational Sciences (NCATS) and funds (Contract 7SN91019D00024) from the National Cancer Institute (NCI) and National Institutes of Health (NIH).

Notes

The authors declare no competing financial interest.

ACKNOWLEDGMENTS

We thank Hannah Ambrose, Matt Drew, Peter Frank, Shelley Perkins, Amanda Seabolt, Min Hong, Ashley Mitchell, Zoe Putman, Matt Smith, and Vanessa Wall from the Protein Expression Laboratory at the Frederick National Laboratory for cloning and protein expression support.

REFERENCES

- (1) Hammond, J.; Leister-Tebbe, H.; Gardner, A.; Abreu, P.; Bao, W.; Wisemandle, W.; Baniecki, M.; Hendrick, V. M.; Damle, B.; Simon-Campos, A.; Pypstra, R.; Rusnak, J. M. Oral Nirmatrelvir for High-Risk, Nonhospitalized Adults with Covid-19. *N. Engl. J. Med.* **2022**, *386* (15), 1397–1408.
- (2) Robson, F.; Khan, K. S.; Le, T. K.; Paris, C.; Demirbag, S.; Barfuss, P.; Rocchi, P.; Ng, W. L. Coronavirus RNA Proofreading: Molecular Basis and Therapeutic Targeting. *Mol. Cell* **2020**, *79* (5), 710–727.
- (3) Tahir, M. Coronavirus genomic nsp14-ExoN, structure, role, mechanism, and potential application as a drug target. *J. Med. Virol* **2021**, *93* (7), 4258–4264.
- (4) Chen, Y.; Cai, H.; Pan, J.; Xiang, N.; Tien, P.; Ahola, T.; Guo, D. Functional screen reveals SARS coronavirus nonstructural protein nsp14 as a novel cap N7 methyltransferase. *Proc. Natl. Acad. Sci. U.S.A.* **2009**, *106* (9), 3484–3489.
- (5) Ogando, N. S.; Zevenhoven-Dobbe, J. C.; van der Meer, Y.; Bredenbeek, P. J.; Posthuma, C. C.; Snijder, E. J. The Enzymatic Activity of the nsp14 Exoribonuclease Is Critical for Replication of MERS-CoV and SARS-CoV-2. *J. Virol* **2020**, *94* (23), No. e01246-20.
- (6) Baddock, H. T.; Brolih, S.; Yosaatmadja, Y.; Ratnaweera, M.; Bielinski, M.; Swift, L. P.; Cruz-Migoni, A.; Fan, H.; Keown, J. R.; Walker, A. P.; Morris, G. M.; Grimes, J. M.; Fodor, E.; Schofield, C. J.; Gileadi, O.; McHugh, P. J. Characterization of the SARS-CoV-2 ExoN (nsp14ExoN-nsp10) complex: implications for its role in viral genome stability and inhibitor identification. *Nucleic Acids Res.* **2022**, *50* (3), 1484–1500.
- (7) Ma, Y.; Wu, L.; Shaw, N.; Gao, Y.; Wang, J.; Sun, Y.; Lou, Z.; Yan, L.; Zhang, R.; Rao, Z. Structural basis and functional analysis of the SARS coronavirus nsp14-nsp10 complex. *Proc. Natl. Acad. Sci. U.S.A.* **2015**, *112* (30), 9436–9441.
- (8) Imprachim, N.; Yosaatmadja, Y.; Newman, J. A. Crystal structures and fragment screening of SARS-CoV-2 NSP14 reveal details of exoribonuclease activation and mRNA capping and provide starting points for antiviral drug development. *Nucleic Acids Res.* **2023**, *51* (1), 475–487.
- (9) Moeller, N. H.; Shi, K.; Demir, O.; Belica, C.; Banerjee, S.; Yin, L.; Durfee, C.; Amaro, R. E.; Aihara, H. Structure and dynamics of SARS-CoV-2 proofreading exoribonuclease ExoN. *Proc. Natl. Acad. Sci. U.S.A.* **2022**, *119* (9), No. e2106379119.
- (10) Jones, A. N.; Mourao, A.; Czarna, A.; Matsuda, A.; Fino, R.; Pyrc, K.; Sattler, M.; Popowicz, G. M. Characterization of SARS-CoV-2 replication complex elongation and proofreading activity. *Sci. Rep.* **2022**, *12* (1), No. 9593.
- (11) Zaffagni, M.; Harris, J. M.; Patop, I. L.; Pamudurti, N. R.; Nguyen, S.; Kadener, S. SARS-CoV-2 Nsp14 mediates the effects of viral infection on the host cell transcriptome. *eLife* **2022**, *11*, No. e71945.
- (12) Asthana, A.; Corona, A.; Shin, W. J.; Kwak, M. J.; Gaughan, C.; Tramontano, E.; Jung, J. U.; Schobert, R.; Jha, B. K.; Silverman, R. H.; Biersack, B. Analogs of the Catechol Derivative Dynasore Inhibit HIV-1 Ribonuclease H, SARS-CoV-2 nsp14 Exoribonuclease, and Virus Replication. *Viruses* **2023**, *15* (7), 1539.
- (13) Canal, B.; McClure, A. W.; Curran, J. F.; Wu, M.; Ulferts, R.; Weissmann, F.; Zeng, J.; Bertolin, A. P.; Milligan, J. C.; Basu, S.; Drury, L. S.; Deegan, T. D.; Fujisawa, R.; Roberts, E. L.; Basier, C.; Labib, K.; Beale, R.; Howell, M.; Diffley, J. F. X. Identifying SARS-CoV-2 antiviral compounds by screening for small molecule inhibitors of nsp14/nsp10 exoribonuclease. *Biochem. J.* **2021**, *478* (13), 2445–2464.

- (14) Wang, X.; Sacramento, C. Q.; Jockusch, S.; Chaves, O. A.; Tao, C.; Fintelman-Rodrigues, N.; Chien, M.; Temerozo, J. R.; Li, X.; Kumar, S.; Xie, W.; Patel, D. J.; Meyer, C.; Garzia, A.; Tuschl, T.; Bozza, P. T.; Russo, J. J.; Souza, T. M. L.; Ju, J. Combination of antiviral drugs inhibits SARS-CoV-2 polymerase and exonuclease and demonstrates COVID-19 therapeutic potential in viral cell culture. *Commun. Biol.* **2022**, *5* (1), 154.
- (15) Rona, G.; Zeke, A.; Miwatani-Minter, B.; de Vries, M.; Kaur, R.; Schinlever, A.; Garcia, S. F.; Goldberg, H. V.; Wang, H.; Hinds, T. R.; Bailly, F.; Zheng, N.; Cotelle, P.; Desmaele, D.; Landau, N. R.; Dittmann, M.; Pagano, M. The NSP14/NSP10 RNA repair complex as a Pan-coronavirus therapeutic target. *Cell Death Differ.* **2022**, *29* (2), 285–292.
- (16) Hernández, S.; Feracci, M.; De Jesus, C. T.; El Kazzi, P.; Kaci, R.; Garlatti, L.; Mondielli, C.; Bailly, F.; Cotelle, P.; Touret, F.; de Lamballerie, X.; Coutard, B.; Decroly, E.; Canard, B.; Ferron, F.; Alvarez, K. Identification of potent inhibitors of arenavirus and SARS-CoV-2 exoribonucleases by fluorescence polarization assay. *Antivir. Res.* **2022**, *204*, No. 105364.
- (17) Ahmed-Belkacem, R.; Hausdorff, M.; Delpal, A.; Sutto-Ortiz, P.; Colmant, A. M. G.; Touret, F.; Ogando, N. S.; Snijder, E. J.; Canard, B.; Coutard, B.; Vasseur, J. J.; Decroly, E.; Debart, F. Potent Inhibition of SARS-CoV-2 nsp14 N7-Methyltransferase by Sulfonamide-Based Bisubstrate Analogues. *J. Med. Chem.* **2022**, *65* (8), 6231–6249.
- (18) Ahmed-Belkacem, R.; Troussier, J.; Delpal, A.; Canard, B.; Vasseur, J. J.; Decroly, E.; Debart, F. N-Arylsulfonamide-based adenosine analogues to target RNA cap N7-methyltransferase nsp14 of SARS-CoV-2. *RSC Med. Chem.* **2024**, *15* (3), 839–847.
- (19) Hausdorff, M.; Delpal, A.; Barelier, S.; Nicollet, L.; Canard, B.; Touret, F.; Colmant, A.; Coutard, B.; Vasseur, J. J.; Decroly, E.; Debart, F. Structure-guided optimization of adenosine mimetics as selective and potent inhibitors of coronavirus nsp14 N7-methyltransferases. *Eur. J. Med. Chem.* **2023**, *256*, No. 115474.
- (20) Otava, T.; Sala, M.; Li, F.; Fanfrlik, J.; Devkota, K.; Perveen, S.; Chau, I.; Pakarian, P.; Hobza, P.; Vedadi, M.; Boura, E.; Nencka, R. The Structure-Based Design of SARS-CoV-2 nsp14 Methyltransferase Ligands Yields Nanomolar Inhibitors. *ACS Infect. Dis.* **2021**, *7* (8), 2214–2220.
- (21) Samrat, S. K.; Bashir, Q.; Zhang, R.; Huang, Y.; Liu, Y.; Wu, X.; Brown, T.; Wang, W.; Zheng, Y. G.; Zhang, Q. Y.; Chen, Y.; Li, Z.; Li, H. A universal fluorescence polarization high throughput screening assay to target the SAM-binding sites of SARS-CoV-2 and other viral methyltransferases. *Emerg. Microbes Infect.* **2023**, *12* (1), No. 2204164.
- (22) Basu, S.; Mak, T.; Ulferts, R.; Wu, M.; Deegan, T.; Fujisawa, R.; Tan, K. W.; Lim, C. T.; Basier, C.; Canal, B.; Curran, J. F.; Drury, L. S.; McClure, A. W.; Roberts, E. L.; Weissmann, F.; Zeisner, T. U.; Beale, R.; Cowling, V. H.; Howell, M.; Labib, K.; Diffley, J. F. X. Identifying SARS-CoV-2 antiviral compounds by screening for small molecule inhibitors of Nsp14 RNA cap methyltransferase. *Biochem. J.* **2021**, *478* (13), 2481–2497.
- (23) Kasprzyk, R.; Spiewla, T. J.; Smietanski, M.; Golojuch, S.; Vangeel, L.; De Jonghe, S.; Jochmans, D.; Neyts, J.; Kowalska, J.; Jemielity, J. Identification and evaluation of potential SARS-CoV-2 antiviral agents targeting mRNA cap guanine N7-Methyltransferase. *Antivir. Res.* **2021**, *193*, No. 105142.
- (24) Hsiao, K.; Zegzouti, H.; Goueli, S. High throughput bioluminescent assay to characterize and monitor the activity of SARS-CoV-2 methyltransferases. *PLoS One* **2022**, *17* (11), No. e0274343.
- (25) Hanson, Q. M.; Hoxie, N.; Shen, M.; Guo, H.; Cho, I. J.; Chakraborty, I.; Aragon, B. M.; Rai, G.; Patnaik, S.; Janiszewski, J. S.; Hall, M. D. Target Class Profiling of Small-Molecule Methyltransferases. *ACS Chem. Biol.* **2023**, *18* (4), 969–981.
- (26) Chen, C. Z.; Shinn, P.; Itkin, Z.; Eastman, R. T.; Bostwick, R.; Rasmussen, L.; Huang, R.; Shen, M.; Hu, X.; Wilson, K. M.; Brooks, B. M.; Guo, H.; Zhao, T.; Klump-Thomas, C.; Simeonov, A.; Michael, S. G.; Lo, D. C.; Hall, M. D.; Zheng, W. Drug Repurposing Screen for Compounds Inhibiting the Cytopathic Effect of SARS-CoV-2. *Front. Pharmacol.* **2020**, *11*, No. 592737.
- (27) Huang, R.; Zhu, H.; Shinn, P.; Ngan, D.; Ye, L.; Thakur, A.; Grewal, G.; Zhao, T.; Southall, N.; Hall, M. D.; Simeonov, A.; Austin, C. P. The NCATS Pharmaceutical Collection: a 10-year update. *Drug Discovery Today* **2019**, *24* (12), 2341–2349.
- (28) Taylor, T.; Denison, J. P.; Esposito, D. Optimizing Expression and Solubility of Proteins in *E. coli* Using Modified Media and Induction Parameters. *Methods Mol. Biol.* **2017**, *1586*, 65–82.
- (29) Studier, F. W. Protein production by auto-induction in high density shaking cultures. *Protein Expr. Purif.* **2005**, *41* (1), 207–234.
- (30) Smith, M.; Hernandez, J. S.; Messing, S.; Ramakrishnan, N.; Higgins, B.; Mehalko, J.; Perkins, S.; Wall, V. E.; Grose, C.; Frank, P. H.; Cregger, J.; Le, P. V.; Johnson, A.; Sherekar, M.; Pagonis, M.; Drew, M.; Hong, M.; Widmeyer, S. R. T.; Denison, J. P.; Snead, K.; Poon, I.; Waybright, T.; Champagne, A.; Esposito, D.; Jones, J.; Taylor, T.; Gillette, W. Producing recombinant proteins in *Vibrio natriegens*. *Microb. Cell Fact.* **2024**, *23* (1), 208.
- (31) Kopra, K.; Vuorinen, E.; Abreu-Blanco, M.; Wang, Q.; Eskonen, V.; Gillette, W.; Pulliainen, A. T.; Holderfield, M.; Härmä, H. Homogeneous Dual-Parametric-Coupled Assay for Simultaneous Nucleotide Exchange and KRAS/RAF-RBD Interaction Monitoring. *Anal. Chem.* **2020**, *92* (7), 4971–4979.
- (32) Waskom, M. L. seaborn: statistical data visualization. *J. Open Source Software* **2021**, *6* (60), 3021.
- (33) Hsiao, K.; Zegzouti, H.; Goueli, S. A. Methyltransferase-Glo: a universal, bioluminescent and homogenous assay for monitoring all classes of methyltransferases. *Epigenomics* **2016**, *8* (3), 321–339.
- (34) Jin, X.; Chen, Y.; Sun, Y.; Zeng, C.; Wang, Y.; Tao, J.; Wu, A.; Yu, X.; Zhang, Z.; Tian, J.; Guo, D. Characterization of the guanine-N7 methyltransferase activity of coronavirus nsp14 on nucleotide GTP. *Virus Res.* **2013**, *176* (1–2), 45–52.
- (35) Chen, J.; Zhou, Y.; Wei, X.; Xu, X.; Qin, Z.; Ong, C. P.; Ye, Z. W.; Jin, D. Y.; Boitrel, B.; Yuan, S.; Chan, J. F.; Li, H.; Sun, H. Development of Pan-Anti-SARS-CoV-2 Agents through Allosteric Inhibition of nsp14/nsp10 Complex. *ACS Infect. Dis.* **2024**, *10* (3), 858–869.
- (36) Liu, C.; Shi, W.; Becker, S. T.; Schatz, D. G.; Liu, B.; Yang, Y. Structural basis of mismatch recognition by a SARS-CoV-2 proofreading enzyme. *Science* **2021**, *373* (6559), 1142–1146.